Thickness-dependent glass transition temperature and charge mobility in cross-linked polyfluorene thin films

Dan Liu, Hui Qin, Jinghui Zhang, and Tao Wang*
School of Materials Science and Engineering, Wuhan University of Technology, Wuhan 430070, China
(Received 19 July 2016; published 4 November 2016)

We report thickness-dependent glass transition temperature (T_g) and charge mobility in cross-linked thin films made of conjugated polymer poly(9,9-dioctylfluorene-co-*N*-(4-butylphenyl)diphenylamine) (TFB). Monotonic T_g depressions with reducing film thickness in thermally and UV cross-linked TFB thin films supported on Si-SiOx substrates are observed through ellipsometry measurements, suggesting that a surface mobile layer with enhanced chain dynamics still exists in cross-linked TFB thin films, even with a high cross-linking percentage. Data fitting using a three-layer model shows that the T_g in the interface, bulk and surface layer both increases with increasing cross-linking, while the thickness of the interface and surface layer increases and reduces, respectively. Cross-linking of TFB thin film generates traps that hinder charge transport and consequently reduce charge mobility. The charge mobility converges in thick (>140 nm) and thin (<40 nm) TFB films but shows strong thickness dependence in between, reducing from 4.0×10^{-4} cm^2/V s in a 180-nm film to 0.1×10^{-4} cm^2/V s in a 20-nm thin film.

DOI: 10.1103/PhysRevE.94.052503

I. INTRODUCTION

Many physical properties of polymers confined in thin film geometry have been found to deviate from their bulk counterparts, for example, glass transition temperature (T_g), viscosity, molecular mobility, and so on [1–4]. Among these physical properties, the T_g in saturated polymer thin films have been widely studied by experimental and computational approaches [5–7]. Although controversial reports can be found in the literature, it is largely agreed in the soft matter physics community that T_g and chain dynamics deviations in polymer thin films are genuine [8,9]. This conclusion has been verified by experimental results carried out using different techniques, including spectroscopic ellipsometry (SE) [1,2], dielectric relaxation [10], fluorescence intensity [11], X-ray reflectivity [12], positron annihilation lifetime spectroscopy (PALS) [13,14], neutron scattering [15–17], and local thermal analysis [18]. The thickness and substrate dependent T_g deviations of polymer thin films originate from the competition between surface and interface modified chain dynamics that virtually divide a thin film into several vertically heterogeneous layers [5,19]. The chain dynamics near the free surface region of a thin film are enhanced to reduce T_g, while constrains and interactions near the interface region usually reduce the chain dynamics to increase T_g [20,21].

Conjugated polymers are often made into thin films as part of many electronic and optoelectronic devices [22,23]. These thin films usually have a thickness ranging from several to hundreds of nanometers and are often stacked adjacently with other films. Similar to saturated polymer thin films, the T_g of conjugated polymer thin films also exhibits thickness and substrate dependence [24–27]. The T_g deviations in conjugated polymer thin films have also been explained by surface and interface effects that are well established in the study of saturated polymer thin films [24,25]. Advanced light scattering techniques on conjugated polymer thin films have confirmed that the molecular packing of conjugated polymers in the cross-sectional direction is heterogeneous [28,29]. These morphological differences have been thought to originate from the surface and interface effects [28,29] and may well contribute to the different chain dynamics, T_g deviations, and charge mobilities in these conjugated polymer systems [24]. Although much research has been dedicated to saturated and conjugated polymer thin films, few works have reported the T_g deviation behavior in cross-linked polymer thin films. It is unclear whether the extra bonding in the cross-linked polymer network will diminish the surface effect to reduce chain dynamics near the free surface or whether it will provide extra constrains to polymer chains near the substrate interface.

In this work, we investigate the T_g behaviors in conjugated poly(9,9-dioctylfluorene-co-*N*-(4-butylphenyl) diphenylamine) (TFB) thin films that are cross-linked by thermal and UV approaches. TFB thin films are commonly used in optoelectronic devices, for instance, light-emitting diodes (LEDs), as a hole extraction or injection layer to enhance device efficiency [30]. In these devices, which are made of a stack of multilayers processed from solution casting, cross-linking is often desired to prevent redissolving of a thin film when another layer is cast on top [31]. Thermal annealing under a proper temperature is important in order to bring a positive improvement to device efficiency [32]. Our results here show that T_g depression with reducing film thickness still exists in cross-linked TFB thin films supported on a Si-SiOx substrate, even at a high cross-linking percentage. Cross-linking reduces charge mobility in TFB thin films as a result of trap generation, and a general thickness-dependent charge mobility is observed in both pristine and cross-linked TFB thin films.

II. EXPERIMENT AND METHODS

The conjugated polymer TFB (molecular structure shown in Fig. 1) was obtained from Luminescence Technology Corp. with a M_w of 30 kDa. Si-SiOx supported TFB films were

*twang@whut.edu.cn

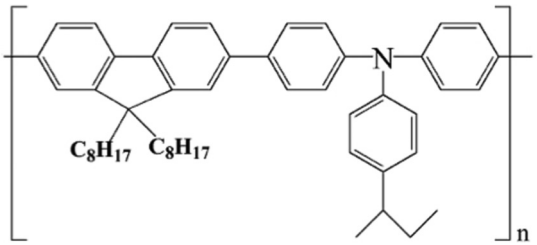

FIG. 1. Molecular structure of the conjugated polymer TFB.

prepared by spin casting at a constant spin speed of 1500 rpm of its chlorobenzene (CB) solutions with concentration ranging from 1.5 to 35 mg/ml, to receive films with thickness from 20 to 200 nm. The Si substrate has a 1.4-nm native silicon oxide layer on top. Each TFB film was held in a vacuum oven at 150 °C for 2 h to minimize residual solvent and stress that were trapped and formed during spin casting. Spectroscopic ellipsometry (M2000D, J. A. Woollam Co., USA) was used to measure the thickness and T_g of all films. The Cauchy model was employed to fit the ellipsometry parameter Ψ and Δ in the wavelength range from 600 to 900 nm, over which the film is optically transparent. Heating and cooling of TFB films were performed in N_2 atmosphere using an Instec heating and cooling setup. During the T_g measurement, the temperature was first heated from room temperature to 200 °C at a rate of 5 °C/min, then cooled to 25 °C at a rate of 2 °C/min. The heating cycle can further remove the residual solvent and stress in TFB films. The thickness vs temperature plot during the cooling cycle was used to determine T_g, which is marked by the intersection of the extrapolated linear fits to the glassy and rubbery regions.

Scanning probe microscopy (SPM) (Solver Next, NT-MDT, Russia) operated with a hybrid module was used to measure the adhesion, deformation, modulus, and stiffness of TFB thin films. The hybrid mode is an oscillatory nonresonant mode that brings the probe and sample into intermittent contact in a vertical oscillation and the induced probe deflection generates a force-distance curve. The attractive wells on the approaching or retracting part of the curve can be employed to measure adhesion and deformation, and the slopes of the curve are related to the stiffness and elastic modulus. Silicon cantilevers (NT-MDT, Russia) with a spring constant of about 5 N m^{-1} and a resonant frequency of 165 kHz were used in all SPM characterizations. All measurements were performed at 25 °C in air.

Thermal cross-linking of a TFB film was performed by adding 4 wt % cross-linking agent dicumyl peroxide (DCP) into the CB solution of TFB. After spin casting, the films were held in a vacuum oven at 80 °C for 12 h, then heated to 125, 140, and 160 °C, respectively, and held for 4 or 12 h to allow cross-linking. UV cross-linking was performed by irradiating spin-coated TFB films under a 254-nm UV light for different durations. The cross-linking among TFB molecules is a radical reaction among the alkyl group of the side chains, with radicals generated either by decomposition of the cross-linker DCP, or cleavage of the C-H bonds (with an energy around 4.3 eV) under the 254-nm UV light (with an energy around 4.9 eV). The gel fraction after cross-linking was determined by comparing TFB thickness changes after sufficient CB solvent soaking until no further thickness reduction of the film was found.

The charge carrier (hole) mobilities of TFB films were determined from the dark *J-V* curves of hole-only devices glass-indium tin oxide (ITO)-poly(3,4-ethylenedioxythiophene):poly (styrene sulfonate) (PEDOT:PSS)-TFB-Au following the space charge limited current (SCLC) transport method. In our hole-only device, a 40-nm-thick PEDOT:PSS was first spin-coated onto the ITO glass at 5000 rpm for 30 s. Then a TFB CB solution with different concentrations (1.5–35 mg/ml) was spin-coated onto the PEDOT:PSS layer. A 30-nm-thick Au cathode was deposited at a rate of 0.5 Å/s on top of TFB via thermal evaporation, under the vacuum of at least 1×10^{-7} Torr.

III. RESULTS AND DISCUSSION

Polymer TFB contains rigid benzene rings on the conjugated backbone, as well as flexible alkyl side chains. The nitrogen atom in the backbone also renders the TFB molecule the possibility to twist its conformation upon cross-linking. The cross-linking of TFB films by thermal and UV treatments was examined by measuring the gel fraction and mechanical properties of the films. Before cross-linking, a TFB film can be easily dissolved by immerging into a CB solution. However, the cross-linked TFB films by either thermal or UV cross-linking cannot be completely dissolved anymore and also won't delaminate from the substrate, even after soaking in CB for 10 days. The gel fraction generally increases with the temperature and duration during thermal cross-linking, as well as the irradiation time during UV cross-linking (in air or N_2). The gel fraction was only 46.1% upon thermal cross-linking at 140 °C for 4 h, and increased to over 90% when the cross-linking was performed at 160 °C for 12 h. As can be seen from Tables I and II, UV cross-linking is more efficient compared with thermal cross-linking, and the irradiation time is substantially shorter to reach the same gel fraction in a TFB thin film.

The occurrence of cross-linking in TFB films can also be justified from the changes of mechanical properties as examined by SPM. The mechanical constants extracted from the force-distance mapping on TFB thin films having the same thickness of 150 nm are compared. Figure 2 shows the Gaussian distribution of mechanical constants, including stiffness, modulus, deformation, and adhesion, of TFB films having

TABLE I. The mechanical constants of 150-nm TFB films upon thermal cross-linking

Cross-linking treatment	Gel fraction (%)	Stiffness (N m^{-1})	Modulus (MPa)	Deformation (nm)	Adhesion (pN)
Pristine	0	1.62 ± 0.26	54.2 ± 18.3	9.9 ± 3.2	26.9 ± 3.8
125 °C 4 h	15.2	3.43 ± 0.31	72.2 ± 18.9	7.2 ± 2.5	18.0 ± 2.0
160 °C 12 h	90.6	4.39 ± 0.28	136.6 ± 46.5	3.3 ± 1.0	10.5 ± 1.2

TABLE II. Fitting parameters from the thickness-dependent T_g depression of thermally and UV cross-linked TFB films using the three-layer model in Eq. (2).

Cross-linking treatment	Gel fraction (%)	$T_g^{\text{interface}}$(°C)	T_g^{bulk}(°C)	T_g^{surface}(°C)	h_1(nm)	h_2(nm)	χ^2
Pristine	0	158.0	146.4	128.0	3.4	22.9	0.84
140 °C 4 h	46.1	164.3	154.1	130.1	4.5	19.0	2.60
160 °C 4 h	65.7	163.7	154.7	130.0	4.4	19.8	0.66
160 °C 12 h	90.6	175.1	166.6	134.0	12.0	14.0	3.20
UV 4 min in air	25.9	160.9	148.3	129.5	3.4	18.5	1.23
UV 12 min in air	44.9	167.3	150.8	130.5	4.0	15.3	0.98
UV 28 min in air	82.0	170.0	162.5	132.6	8.6	14.4	0.54
UV 4 min in N_2	20.1	157.2	146.4	127.0	3.7	21.4	2.63
UV 12 min in N_2	31.2	159.1	150.2	128.9	3.7	20.5	1.65
UV 28 min in N_2	50.1	159.7	153.1	129.0	4.2	16.7	0.86

three different gel fractions. Table I summarizes the peak values and error bars of these mechanical constants. Under the temperature of 25 °C, the pristine TFB film has the lowest stiffness (1.62 ± 0.26 N m^{-1}) and modulus (54.2 ± 18.3 MPa), but the highest deformation (9.9 ± 3.2 nm) and adhesion (26.9 ± 3.8 pN). With increasing gel fraction, the stiffness and modulus rise, and the deformation and adhesion reduce. When the gel fraction is much higher at 90.6%, the stiffness and modulus reach 4.39 ± 0.28 N m^{-1} and 136.6 ± 46.5 MPa, respectively, and the deformation and adhesion decrease to 3.3 $\pm$ 1.0 nm and 10.5 $\pm$ 1.2 pN, respectively. Similar tendencies on the mechanical constants of UV cross-linked TFB films were observed (data not shown). Upon cross-linking among the alkyl side chains, more constrains are generated among

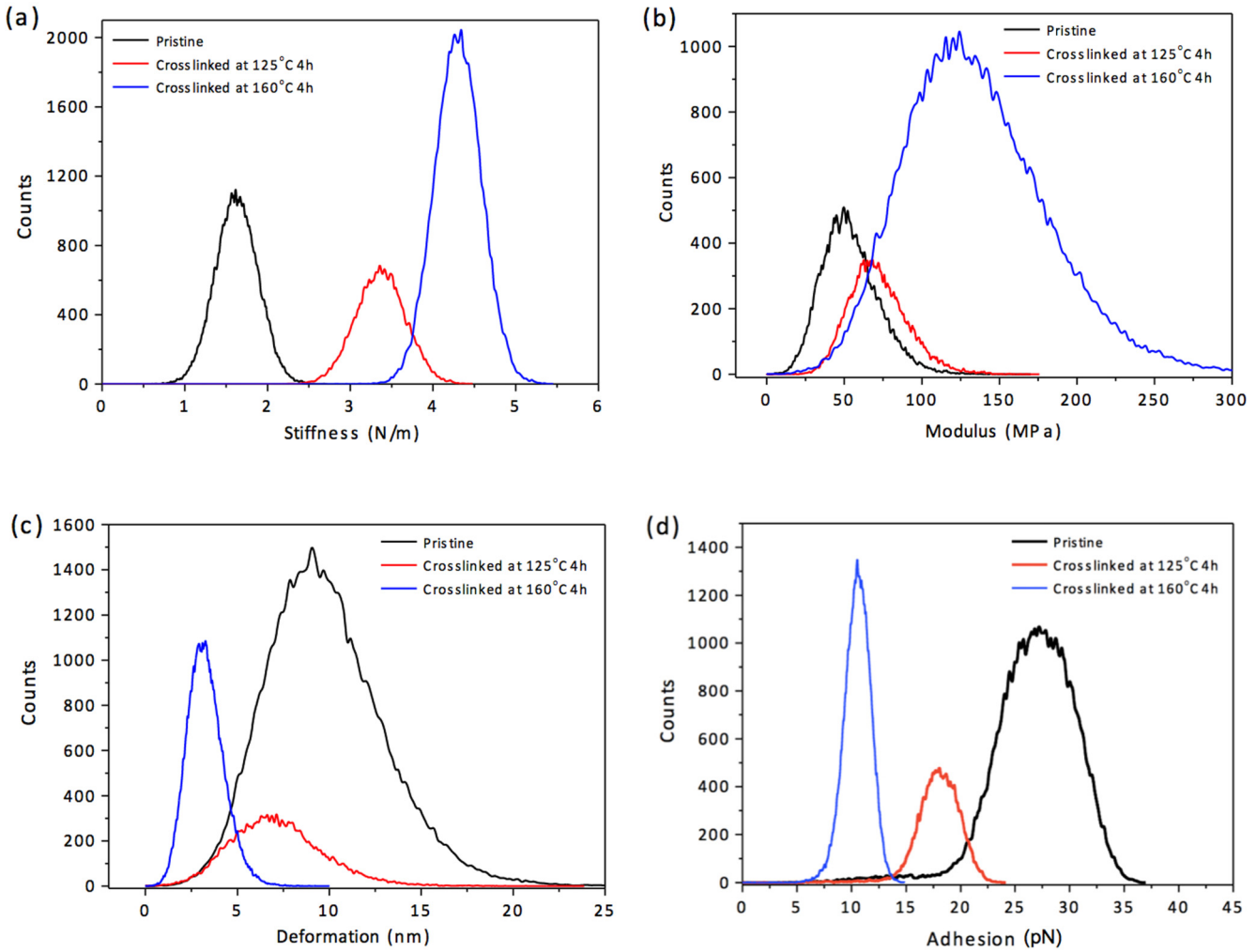

FIG. 2. Gaussian distributions of mechanical constants of a 150-nm TFB thin film under different thermal cross-linking conditions: (a) stiffness; (b) modulus; (c) deformation; and (d) adhesion.

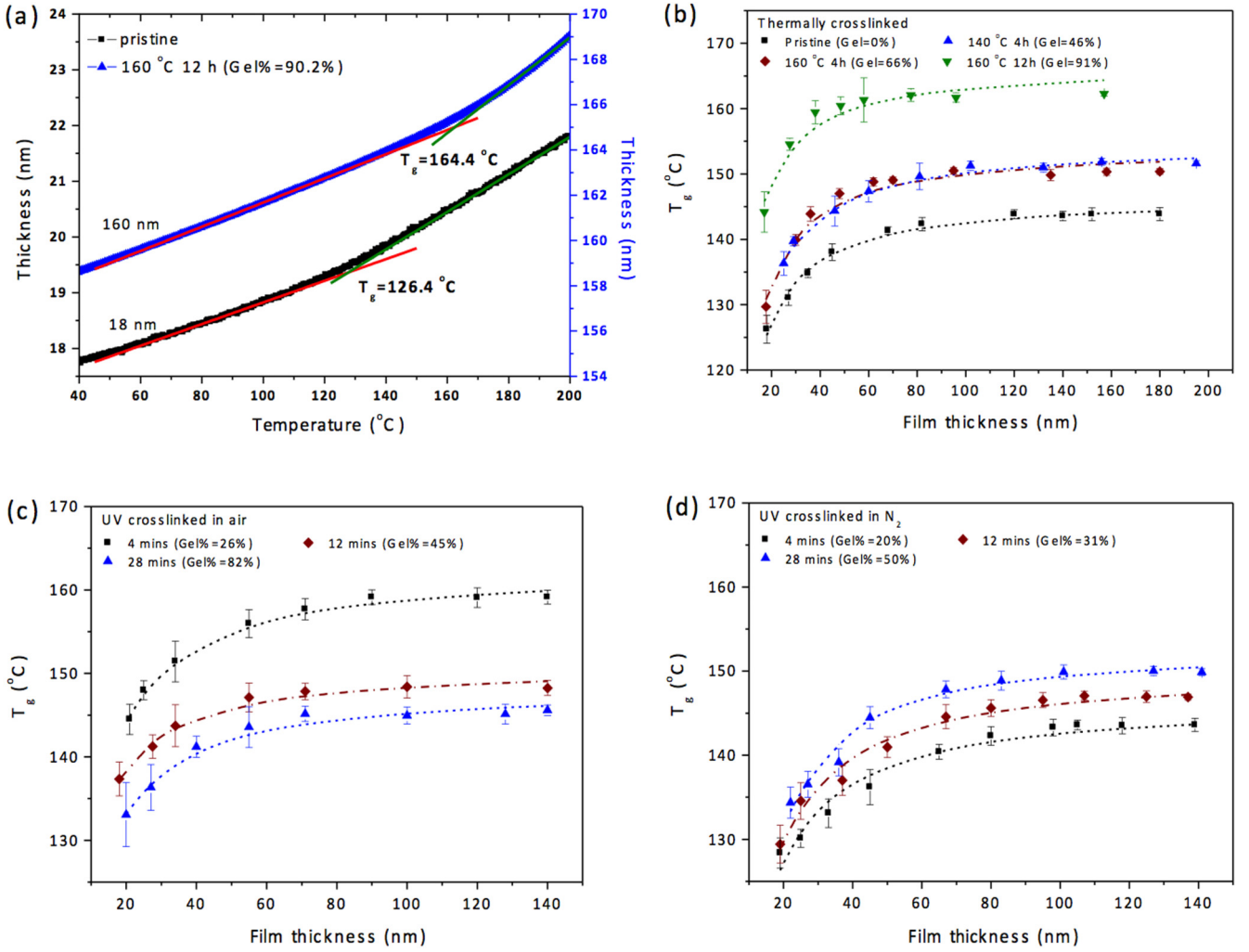

FIG. 3. (a) Thickness vs temperature plots of two TFB films with different thicknesses and gel fractions supported on Si-SiOx substrate. (b) T_g depression of pristine and thermally cross-linked TFB films having different gel fractions with reducing film thickness. (c, d) The T_g depressions of TFB films having different gel fractions after UV cross-linking in air and N_2, respectively.

TFB chains, leading to reduced flexibility and consequently enhanced stiffness and modulus but reduced deformation and adhesion. As SPM probes the surface part of a thin film, the changes of the mechanical constants certainly suggest that the surface regions are cross-linked, while it is inconclusive by this technique to infer that the same is true for the cross-linking in the bulk or interface layers away from the surface region.

Cross-linking also elevates the average T_g of a TFB thin film, as can be determined from our SE measurements. With a film thickness of about 160 nm, the T_g of a TFB film having a gel fraction of 90.6% (achieved by thermal cross-linking at 160 °C for 12 h) is 164.4 °C [see Figs. 3(a) and 3(b)]. This is significantly higher than that of 143 °C of the pristine TFB film [see Fig. 3(b)]. For TFB films with different gel fractions, a higher T_g was also obtained compared with the pristine TFB film of similar thickness. This can be observed in cross-linked TFB films by either thermal or UV cross-linking. By comparing Figs. 3(c) with 3(d), it seems that for the same irradiation time, UV cross-linking in air is more efficient to raise the gel fraction in the TFB films and increase the film T_g.

Our previous work has observed thickness-dependent T_g deviations in pristine TFB films supported on Si-SiOx, with monotonic T_g depression observed in films thinner than *ca.* 60 nm [25]. This is confirmed again in this work through TFB films having a different molecular weight [see Fig. 3(b)]. More importantly, monotonic thickness-dependent T_g deviation is observed here in all TFB films having low and high gel fractions by either thermal or UV cross-linking, as shown in Figs. 3(b)–3(d). When the film thickness is over 80 nm thick, T_g converges to a plateau in all TFB films. A general T_g reduction up to 15 °C can be determined in very thin cross-linked TFB films around 20 nm thick. We note here that the T_g of a polymer film thinner than 10 nm cannot be accurately determined by SE measurements, as the two linear regions corresponding to the glassy and rubbery states, respectively, in the thickness-temperature plot will disappear [33]. However, a 20-nm TFB film is thick enough with obvious linear glassy and rubbery regions to allow T_g to be determined with confidence [see Fig. 3(a)]. We note that T_g depression with reducing film thickness in cross-linked polystyrene thin films was reported by Jin and Torkelson recently, although the bulk T_g increases

with increased cross-linking [34]. The T_g reduction upon confinement in cross-linked PS films is even larger after cross-linking, and this is correlated with the increased bulk fragility due to the enhanced coupling between the relaxing units [34].

It is generally believed that T_g of a polymer thin film is affected by its free surface as well as the interface between its substrate. The enhanced chain dynamic at the free surface will reduce T_g [20,35]. Strong interactions at the polymer-substrate interface will constrain the chain dynamic and elevate T_g, while weak interactions make negligible impacts on the chain dynamic and T_g [16,36]. The average T_g of the whole thin film results from the competition between the interface and free surface effects [24]. Since the T_g depression in ultrathin films is largely due to the surface effect, our results here indicate that the constrains between TFB molecules due to cross-linking will not significantly restrict chain dynamics at the surface. The surface effect still dominates and outweighs constrains due to cross-linking and interface effects, leading to a reduced average T_g when the film is thinner than the critical thickness around 80 nm.

These surface and interface effects have been incorporated into various layered models that virtually divide a thin film into several vertically heterogeneous layers, each having different chain dynamics and T_g [1,25,37,38]. In our previous work [25], we have proposed a three-layer model [expressed by Eq. (1)] based on the well-accepted Keddie-Jones-Cory model [1]:

$$T_g(h) = \frac{h - h_1}{h} T_g^{\text{bulk}} \left[1 - \left(\frac{\gamma}{h}\right)^{\delta}\right] + \frac{h_1}{h} T_g^{\text{interface}}. \quad (1)$$

Here, γ and h_1 empirically represent the thickness of the surface layer (i.e., interface with air) and interface layer (i.e., interface with the substrate), respectively. δ is a fitting constant that will vary as a result of correlation with other parameters in Eq. (1), h is the total thickness of the thin film, and $T_g{}^{\text{interface}}$ defines the T_g of the interface layer. This three-layer model has been demonstrated to be able to fit both monotonic and nonmonotonic T_g deviation behaviors in conjugated polymer thin films [25].

We found that our data plots in Figs. 3(b)–3(d) can be well fitted using this equation. Here we further modify Eq. (1) to the following Eq. (2), so that the T_g of the surface, bulk, and interface layers can all be found in one model, as well as the thickness of each layer:

$$T_g(h) = \frac{h - (h_1 + h_2)}{h} T_g^{\text{bulk}} + \frac{h_2}{h} T_g^{\text{surface}} + \frac{h_1}{h} T_g^{\text{interface}}. \quad (2)$$

Here, h_1 and h_2 represent the thickness of the interface and surface layer, respectively, h is the total thickness of the thin film, and $T_g{}^{\text{surface}}$ and $T_g{}^{\text{interface}}$ define the T_g of the surface and interface layer.

The dashed gray lines in Figs. 3(b)–3(d) are the fitted curves using the three-layer model expressed by Eq. (2), showing that our experimental data can all be well fitted with a low χ^2. Table II lists the fitting parameters of Figs. 3(b)–3(d). Figure 4 plots the variations of T_g and layer thickness as a function of gel fraction (modified by either thermal or UV cross-linking) that are summarized in Table II. As can be seen from Fig. 4(a), $T_g{}^{\text{bulk}}$ and $T_g{}^{\text{interface}}$ both increase as the gel fraction increases, which confirms the reduced chain dynamics, especially in the bulk and interface regions after cross-linking. The $T_g{}^{\text{surface}}$ also increases but at a much smaller rate compared with the other two in Fig. 4(a). The changes of mechanical constants (Fig. 2) by SPM measurements already suggest that this region has been cross-linked. We have also measured the gel fractions of TFB films having different thicknesses that have been cross-linked by the conditions stated in Figs. 3(b)–3(d), and no thickness-dependent gel fraction can be found. For a specific cross-linking treatment, the gel fraction remains constant when film thickness changes (with the variations falling within the error bars), which indicates that the cross-linking is homogeneous in the cross section of a TFB thin film. That is to say, the gel fraction in the surface region would be similar to that in the bulk or interface region. Model fitting also suggests that the thickness of the surface layer is

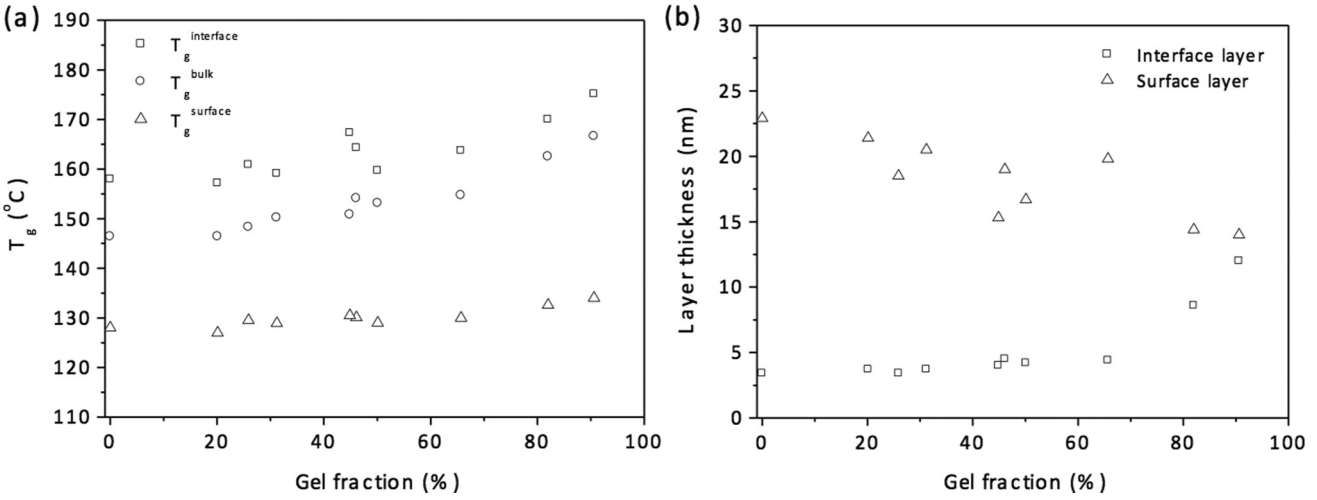

FIG. 4. (a) $T_g{}^{\text{interface}}$, $T_g{}^{\text{bulk}}$, and $T_g{}^{\text{surface}}$ obtained from data fitting using Eq. (2) as a function of gel fraction in cross-linked TFB films. (b) The thickness of the surface (h_2) and interface (h_1) layer obtained from data fitting using Eq. (2) as a function of gel fraction in cross-linked TFB films.

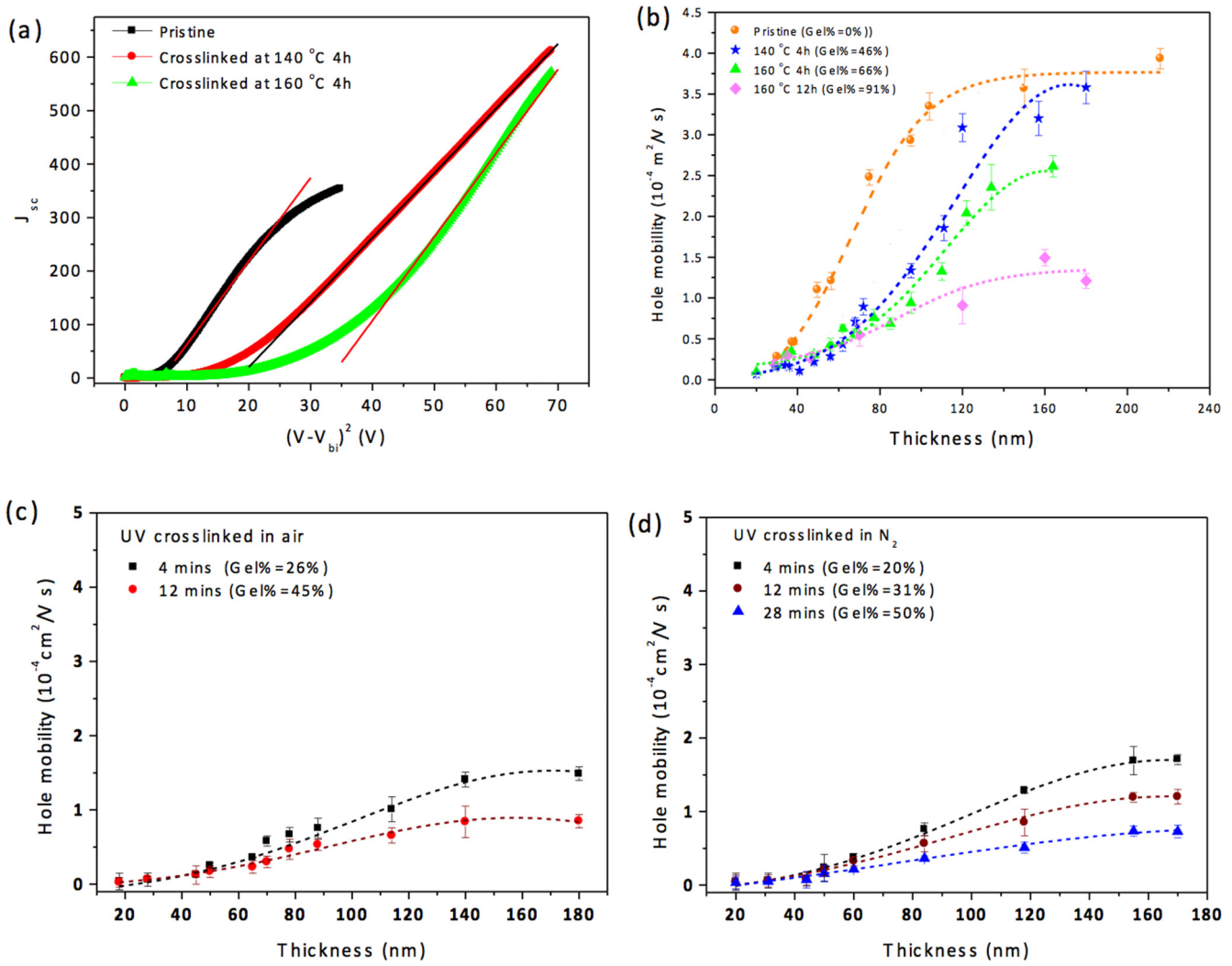

FIG. 5. (a) Dark J-$(V$-$V_{bi})^2$ characteristics of TFB hole-only devices. The thickness of these TFB films is around 60 nm. (b) Thickness-dependent hole mobility of TFB films after different thermal treatments. (c, d) Thickness-dependent hole mobility of TFB films after different UV cross-linking times in air and N_2, respectively. The dashed lines are a guide to the eyes.

much bigger than the interface layer when the gel fraction is low. However, the former reduces and the later increases [see Fig. 4(b)] when the gel fraction increases, reaching a thickness of 14 and 12 nm, respectively, when the gel fraction is 90.6%. When the gel fraction increases, the interface region has increased $T_g^{\text{interface}}$ with a larger volume fraction, leading to the much higher average film T_g, as can be measured by SE in this work. Importantly, however, a surface region with a low T_g^{surface} still exists in the cross-linked TFB film even with high gel fraction.

As the conjugated polymer TFB has relatively high hole mobility and is often prepared into thin films and incorporated into optoelectronic devices such as organic light-emitting diodes, the hole mobility changes in TFB films having different thicknesses, and gel fraction values are investigated next. We extracted the hole mobility of TFB thin films from the dark J-V curves of hole-only devices with the structure glass-ITO-PEDOT:PSS-TFB-Au. Figure 5(a) shows typical dark J-$(V$-$V_{bi})^2$ characteristics of a hole-only device with semiconducting TFB as the active layer. In general, the current density–electric field characterstics can be distinguished into four regions, that is, the Ohmic region, trap-limited region, trap-free voltage limit region, and trap-free SCLC region [39,40]. In the trap-free SCLC region [the linear regions at high voltage fitted with lines in Fig. 5(a)], the out-of-plane charge carrier (hole) mobility follows Eq. (3) [39]:

$$J = \frac{9}{8}\varepsilon\varepsilon_0\mu\frac{(V - V_{bi})^2}{h^3}. \tag{3}$$

Here ε_0 is the permittivity of free space and ε represents the dielectric constant of the conjugated polymer, V and V_{bi} represent applied voltage and the built-in voltage due to the different work functions of electrodes, h is the thickness of the TFB film, and μ is charge mobility.

The hole mobility of TFB films having different thicknesses before and after thermal or UV cross-linking are calculated and summaried in Figs. 5(b)–5(d). Figure 5(b) shows the SCLC hole mobilities of pure and thermally cross-linked TFB films having different thickness. First of all, the hole

mobility is found to decrease with increasing gel fraction when the thickness of the TFB film is similar. It is $3.6 \times 10^{-4}\,\mathrm{cm}^2/\mathrm{V\,s}$ in a 160-nm pristine TFB film but reduces to $\sim 1.2 \times 10^{-4}\,\mathrm{cm}^2/\mathrm{V\,s}$ after thermal cross-linking at 160 °C for 12 h (gel% = 90.6%), which is two times lower. This reduced hole mobility is due to molecule disorder and twists after cross-linking, which generates morphological or energetic traps to hinder charge transport. When the film is thicker than the critical value of 140 nm, a plateau of hole mobility can be obtained, although this plateau value depends on the gel fraction in TFB films. When the film thickness is reduced below this critical value, the TFB hole mobility exhibits thickness dependence and reduces in thinner films, similar to the T_g depression in thinner TFB films. While the enhanced chain dynamics in thinner films will depress the average T_g, they also reduce the structural order of TFB films to decrease the charge mobility. For TFB films thinner than 40 nm, the hole mobility converges without significant changes, although the gel fraction might be different. Figures 5(c) and 5(d) show the hole mobility of UV cross-linked TFB films in air and N_2. Similar conclusions can be drawn for the UV cross-linked TFB films, whose hole mobilities also exhibit thickness and gel fraction dependence. We have presented earlier in Fig. 3 and Table II that UV cross-linking in air is more efficient at increasing the gel fraction and elevating film T_g. The presence of oxygen molecules in air might facilitate the cross-linking process and leads to this end. Here we also compared the hole mobilities of two 180-nm TFB films by UV irradiation in air and N_2, respectively, for the same irradition time. The hole mobilities are around 1.5 and $0.9 \times 10^{-4}\,\mathrm{cm}^2/\mathrm{V\,s}$ after UV irradiation for 4 and 12 min in air, and are slightly higher at 1.7 and $1.2 \times 10^{-4}\,\mathrm{cm}^2/\mathrm{V\,s}$ after UV irradiation for 4 and 12 min in N_2. These results are consistent with the changes in gel fraction and T_g, although the very small variations in these hole mobilities makes it inconclusive.

Conjugated polymers tend to $\pi-\pi$ stack during their solution casting process into thin films. The spin speed during spin coating might lead to different amounts of $\pi-\pi$ stacks in a conjugated polymer thin film and results in the variation of hole mobility [41]. We further investigated the hole mobility of TFB films of the same thickness spun at three conditions: (1) 30 mg/ml at 4000 rpm, (2) 10 mg/ml at 1000 rpm, and (3) 4 mg/ml at 600 rpm. These result in films around 100 nm thick, and possibly different amounts of $\pi-\pi$ stacks in each film. The average hole mobilities of these three TFB films are 3.0, 3.0, and $3.1 \times 10^{-4}\,\mathrm{cm}^2/\mathrm{V\,s}$, respectively. This suggests that different film casting conditions have no influence on the out-of-plane hole mobility of TFB, as TFB in these thin films is in a completely amorphous state without the formation of any π-π stacks during solidification [25]. The results here provide a precise guide for the fabrication and design of high-performance optoelectronic devices with desired charge mobility.

IV. CONCLUSIONS

In conclusion, we have observed deviations of T_g and hole mobility in pristine, UV, and thermally cross-linked conjugated polymer TFB thin films. Monotonic T_g depressions with decreasing film thicknesses were found in pristine TFB films as well as UV and thermally cross-linked TFB thin films supported on Si-SiOx substrate. Fitting of the T_g vs temperature plots using a three-layer model indicates that the T_g of the surface, bulk, and interface layers all increase as cross-linking increases, while the thickness of the surface and interface layer reduces and increases, respectively. The surface layer will not disappear when the TFB film is cross-linked, even with a high gel fraction. The surface layer with enhanced chain dynamics outweighs any constrains from cross-linking and interface effects, and leads to reduced T_g in thinner and cross-linked TFB films. Cross-linking reduces the hole mobility of conjugated TFB thin films due to morphological and energetic traps that hinder charge transport. We also observed a thickness-dependent hole mobility in pristine and cross-linked TFB films. The hole mobility converges in thick (>140 nm) and thin (<40 nm) TFB films but shows strong thickness dependence in between.

ACKNOWLEDGMENTS

This work is supported by the National Natural Science Foundation of China (Grant No. 21504065) and the Fundamental Research Funds for the Central Universities (WUT: 143101003) of China. T.W. also acknowledges support from the Recruitment Program of Global Experts (The Thousand Talents Plan) of China. We also acknowledge reviewers for their especially helpful comments.

[1] J. L. Keddie, R. A. L. Jones, and R. A. Cory, Europhys. Lett. **27**, 59 (1994).
[2] J. L. Keddie, A. L. Richard, and R. A. Cory, Faraday Discuss. **98**, 219 (1994).
[3] C. B. Roth and J. M. Torkelson, Macromolecules **40**, 3328 (2007).
[4] Z. Yang, Y. Fujii, F. K. Lee, C.-H. Lam, and O. K. C. Tsui, Science **328**, 1676 (2010).
[5] J. A. Forrest and K. Dalnoki-Veress, Adv. Colloid Interface Sci. **94**, 167 (2001) .
[6] C. B. Roth and R. Dutcher, J. Electroanal. Chem. **584**, 13 (2005).
[7] R. P. White, C. C. Price, and J. E. G. Lipson, Macromolecules **48**, 4132 (2015).
[8] O. Bäumchen, J. D. McGraw, J. A. Forrest, and K. Dalnoki-Veress, Phys. Rev. Lett. **109**, 055701 (2012).
[9] M. D. Ediger and J. A. Forrest, Macromolecules **47**, 471 (2014).
[10] K. Fukao and Y. Miyamoto, Phys. Rev. E **61**, 1743 (2000).
[11] M. J. Burroughs, S. Napolitano, D. Cangialosi, and R. D. Priestley, Macromolecules **49**, 4647 (2016).
[12] T. Miyazaki, R. Inoue, K. Nishida, and T. Kanaya, Eur. Phys. J. Spec. Top. **141**, 203 (2007).
[13] C. L. Soles, J. F. Douglas, W.-L. Wu, H. Peng, and D. W. Gidley, Macromolecules **37**, 2890 (2004).
[14] Y. C. Jean, R. Zhang, H. Cao, J.-P. Yuan, C.-M. Huang, B. Nielsen, and P. Asoka-Kumar, Phys. Rev. B **56**, R8459 (1997).

[15] R. L. Jones, S. K. Kumar, D. L. Ho, R. M. Briber, and T. P. Russell, Macromolecules **34**, 559 (2001).
[16] E. K. Lin, R. Kolb, S. K. Satija, and W.-L. Wu, Macromolecules **32**, 3753 (1999).
[17] R. Inoue, K. Kawashima, K. Matsui, T. Kanaya, K. Nishida, G. Matsuba, and M. Hino, Phys. Rev. E **83**, 021801 (2011).
[18] D. S. Fryer, P. F. Nealey, and J. J. de Pablo, Macromolecules **33**, 6439 (2000).
[19] H. Qin, D. Liu, and T. Wang, Adv. Mater. Interfaces **3**, 1600084 (2016).
[20] Z. Fakhraai and J. A. Forrest, Science **319**, 600 (2008).
[21] J. A. Torres, P. F. Nealey, and J. J. de Pablo, Phys. Rev. Lett. **85**, 3221 (2000).
[22] G. Ho, H. Meng, S. Lin, S. Horng, C. Hsu, L. Chen, and S. Chang, Appl. Phys. Lett. **85**, 4576 (2004).
[23] L. Chua, J. Zaumseil, J. Chang, E. C. W. Ou, P. K. H. Ho, H. Sirringhaus, and R. H. Friend, Nature (London) **434**, 194 (2005).
[24] T. Wang, A. J. Pearson, A. D. F. Dunbar, P. A. Staniec, D. C. Watters, D. Coles, H. Yi, A. Iraqi, D. G. Lidzey, and R. A. L. Jones, Europ. Phys. J. E **35**, 129 (2012).
[25] D. Liu, R. Osuna Orozco, and T. Wang, Phys. Rev. E **88**, 022601 (2013).
[26] M. Campoy-Quiles, M. Sims, P. G. Etchegoin, and D. D. C. Bradley, Macromolecules **39**, 7673 (2006).
[27] A. Roigé, M. Campoy-Quiles, J. O. Ossó, M. I. Alonso, L. F. Vega, and M. Garriga, Synth. Met. **161**, 2570 (2012).
[28] D. H. Kim, Y. D. Park, Y. Jang, H. Yang, Y. H. Kim, J. I. Han, D. G. Moon, S. Park, T. Chang, C. Chang, M. Joo, C. Y. Ryu, and K. Cho, Adv. Funct. Mater. **15**, 77 (2005).
[29] M. Tong, S. Cho, J. T. Rogers, K. Schmidt, B. B. Y. Hsu, D. Moses, R. C. Coffin, E. J. Kramer, G. C. Bazan, and A. J. Heeger, Adv. Funct. Mater. **20**, 3959 (2010).
[30] T. Wang, Y. Zhang, Y. Yan, C. G. Jones, and D. G. Lidzey, J. Display Tech. **12**, 583 (2016).
[31] J. Lee, H. Han, J. Lee, S. C. Yoon, and C. Lee, J. Mater. Chem. C **2**, 1474 (2014).
[32] M. Shakutsui, H. Matsuura, and K. Fujita, Org. Electron. **10**, 834 (2009).
[33] S. Kawana and R. A. L. Jones, Phys. Rev. E **63**, 021501 (2001).
[34] K. Jin and J. M. Torkelson, Macromolecules **49**, 5092 (2016).
[35] C. J. Ellison and J. M. Torkelson, Nat. Mater. **2**, 695 (2003).
[36] O. K. C. Tsui, T. P. Russell, and C. J. Hawker, Macromolecules **34**, 5535 (2001).
[37] J. H. Kim, J. Jang, and W.-C. Zin, Langmuir **16**, 4064 (2000).
[38] H. Zhou, H. K. Kim, F. G. Shi, B. Zhao, and J. Yota, Microelectron. J. **33**, 221 (2002).
[39] Z. Chiguvare and V. Dyakonov, Phys. Rev. B **70**, 235207 (2004).
[40] M. Arif, M. S. Yun, S. Gangopadhyay, K. Ghosh, L. Fadiga, F. Galbrecht, U. Scherf, and S. Guha, Phys. Rev. B **75**, 195202 (2007).
[41] D. M. DeLongchamp, B. M. Vogel, Y. Jung, M. C. Gurau, C. A. Richter, O. A. Kirillov, J. Obrzut, D. A. Fischer, S. Sambasivan, L. J. Richter, and E. K. Lin, Chem. Mater. **17**, 5610 (2005).